Aerodynamic Characteristics of Rectangular Cross-Sectional Bodies at $M = 0.85$

Asher Sigal*
Technion—Israel Institute of Technology, Haifa, Israel

Wind-tunnel tests of a body having a rectangular cross-section with rounded corners and five interchangeable afterbodies of various tapers are described. The Mach number was 0.85, and the angle of attack varied between −2 and 18 deg. Reduction of the thickness of the afterbody had only a small effect on the normal-force curve slope, in agreement with slender-body theory. Reduction of the width of the afterbody decreased the normal-force curve slope and shifted the center of pressure forward. Afterbody taper enhanced the vortex-induced contribution to the normal force and caused a backward shift of the center of pressure of this contribution.

Nomenclature

A = coefficient in the model for vortex normal force
b = width
B = width of centerbody
B_B = width of base
C_{Af} = forebody axial-force coefficients, contribution of base excluded
C_{At} = total axial-force coefficient
C_{D_c} = crossflow drag coefficient
C_m = pitching-moment coefficient referenced to nose-centerbody interface
C_{m_α} = slope of pitching-moment curve at small angles of attack
C_N = normal-force coefficient
C_{N_α} = slope of normal-force curve at small angles of attack
C_{P_b} = base pressure coefficient
d = reference length, $d = \sqrt{S_R}$
H = thickness of centerbody
H_B = thickness of base
ℓ_1 = length of centerbody and afterbody
ℓ_n = length of the nose
M = Mach number
S_B = base area
S_P = projection area
S_R = reference area, cross-sectional area of centerbody
x = longitudinal coordinate
X_{cp} = center of pressure at small angles of attack, measured from the nose-centerbody interface, positive forward
α = angle of attack
α^v = angle of attack for onset vortex normal force
δ = afterbody taper angle
η = proportionality factor in the expression for crossflow drag
N = nose
B = centerbody
AB = double-taper afterbody
BT = single-taper afterbody

Subscript and Superscript

v = vortex-induced contribution
SB = value obtained from slender-body theory

Introduction

THE interest in the aerodynamic characteristics of bodies having noncircular cross-sections has grown recently because of potential for increased maneuverability and the efficient packaging of subloads. The interest is twofold. The applied aerodynamicist is mainly concerned with data bases, aerodynamic coefficients, and the validity of prediction methods; the fluid dynamicist addresses flow phenomena with emphasis on the formation of vortices at moderate and large angles of attack.[1]

In 1982, the Aerodynamic Laboratory of the Aeronautical Research Center launched an experimental investigation of the aerodynamic characteristics of bodies having square and rectangular cross-sections. Circular bodies having matching fineness ratios were also included for comparison, as described in Ref. 2. The objectives of the present investigation are to obtain wind-tunnel data on the aerodynamics of rectangular bodies, with emphasis on the effects of afterbody geometry on the normal-force and pitching-moment coefficients, and to analyze the results.

Experimental Investigation

The wind-tunnel experiments were carried out in the transonic wind-tunnel of the Aeronautical Research Center of the Technion. This is a closed-cycle, injector-driven facility capable of operating at Mach numbers up to 1.06. The test section is 60-cm wide by 80-cm high and has perforated floor and ceiling.

The cross-section of the model centerbody is rectangular, with a width to thickness ratio of about 1.8. The reference length d equals the square root of the cross-sectional area of the centerbody. The corners of the body are rounded to a radius equal to $0.1\,d$ and the length of the centerbody is $4\,d$. The nose is a tangent rectangular ogive, $1.5\,d$ long. Five interchangeable afterbodies, all of $2d$ length, were tested. One is untapered, namely, a cylindrical extension of the centerbody. Two have a single taper, in thicknesses of 5 and 7 deg, and two have a double taper, in thickness and planform of the same angles. The scheme of the model parts and their dimensions are given in Fig. 1, a picture is shown in Fig. 2, and the main geometrical parameters are summarized in Table 1.

The Mach number of the present tests was 0.85, yielding a unit Reynolds number of 0.145×10^6 per cm. Under these

Received Dec. 14, 1987; revision received May 13, 1988.

*Associate Professor; currently BRL-NRC Research Associate. Member AIAA.

conditions, the boundary layer is mostly turbulent. The angle of attack varied from -2 to 18 deg.

A six-component string balance was used for the measurement of forces and moments. Base pressure was also measured so that the forebody contribution to axial force could be separated from the total force, measured by the balance. A schlieren system was used to visualize the structure of the separated body vortices at angles of attack.

Test Results

Axial Force

The thickness of the base of some afterbodies is smaller than the diameter of the balance. Thus, measured base pressure may not represent undisturbed flight conditions with the same basic geometry. Total axial-force coefficients should only be considered as indications, not accurate values. Table 2 shows a considerable reduction of the total axial-force coefficient at zero angle of attack with increase in afterbody taper. It is apparent that this reduction is caused by the increase in base pressure coefficient, which becomes positive for the double-taper afterbodies. Forebody axial force coefficient is estimated by

$$C_{A_f} = C_{A_t} + \frac{S_B}{S_R} C_{p_b}$$

Table 2 shows that the differences in forebody axial-force coefficient are within the experimental error. No increase was found in forebody axial force due to afterbody taper.

Normal Force and Pitching Moment

Normal-force coefficient curves are presented in Figs. 3a and 3b for afterbodies with single- and double-taper afterbodies,

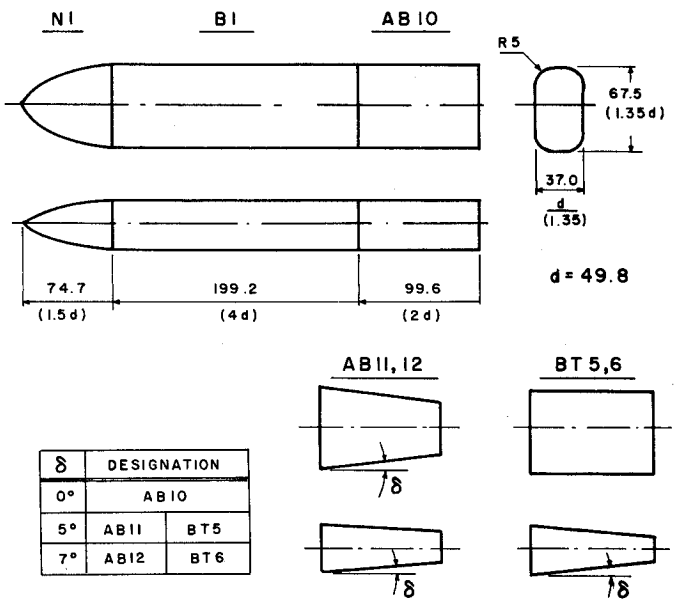

Fig. 1 Geometry of test models.

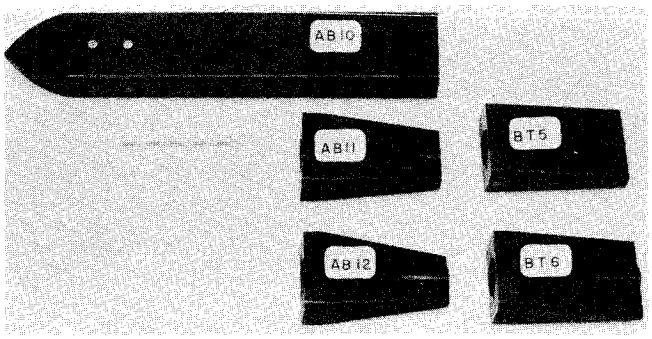

Fig. 2 Photograph of test models.

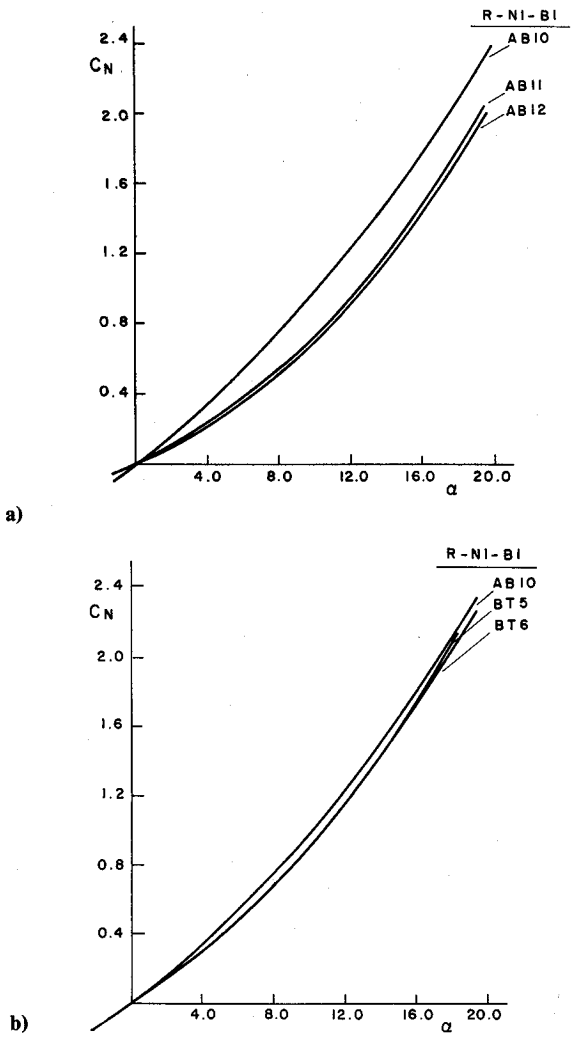

Fig. 3 Test results – normal-force coefficient: a) single-taper afterbodies; b) double-taper afterbodies.

Table 1 Geometrical parameters of the afterbodies

δ		Double taper				Single taper		
0		$AB10$	$l_{AB}/d = 2$, all afterbodies					
5 deg	$AB11$	B_B/B	=	0.74	$BT5$	B_B/B	=	1.0
		H_B/H	=	0.53		H_B/H	=	0.53
		S_B/S_R	=	0.39		S_B/S_R	=	0.53
7 deg	$AB12$	B_B/B	=	0.64	$BT6$	B_B/B	=	1.0
		H_B/H	=	0.34		H_B/H	=	0.34
		S_B/S_R	=	0.21		S_B/S_R	=	0.34

Table 2 Zero angle-of-attack axial-force coefficients

Configuration	C_{A_t}	C_{P_b}	C_{A_f}
$N1 - B1 - AB10$	0.21	−0.10	0.11
$- BT5$	0.13	−0.06	0.10
$- BT6$	0.12	−0.02	0.11
$- AB11$	0.09	0.04	0.11
$- AB12$	0.09	0.10	0.10

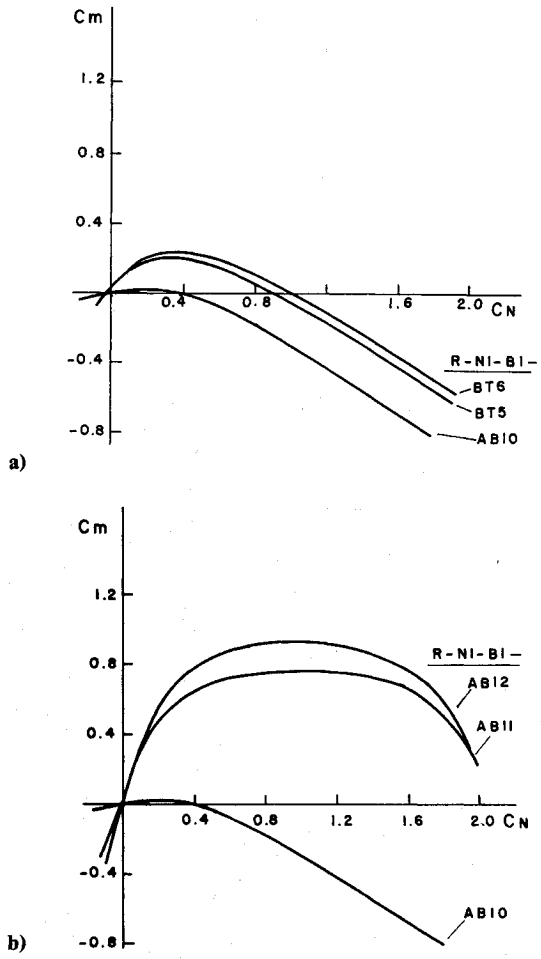

Fig. 4 Test results – pitching-moment coefficient: a) single-taper afterbodies; b) double-taper afterbodies.

Table 3 Comparison of test results at $M = 0.85$ to slender-body theory for configurations with cylindrical afterbodies

Cross section	Rectangular	Circular
C_{N_α}	4.60	2.30
$C_{N_{\alpha SB}}$	3.99	2.00
$C_{N_\alpha}/C_{N_{\alpha SB}}$	1.15	1.15
X_{cp}/d	0.11	0.00
$(X_{cp}/d)_{SB}$	0.83	0.60
$\delta\,(X_{cp}/d)$	−0.72	−0.60

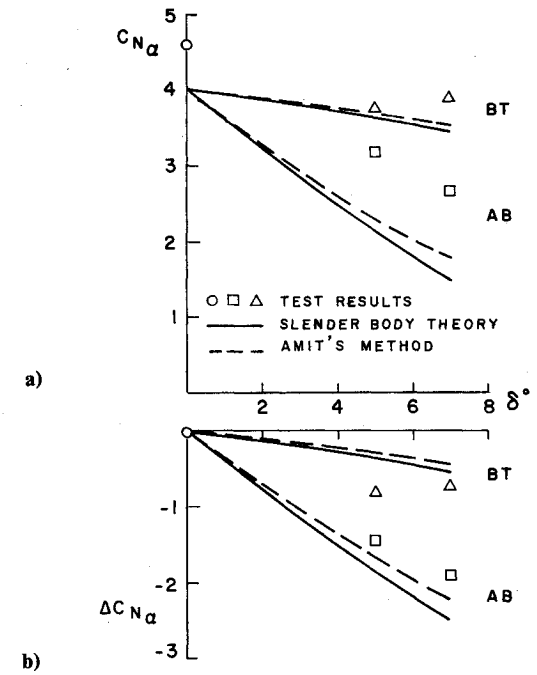

Fig. 5 Normal-force curve slope: a) complete configurations; b) contribution of the afterbody.

respectively. The single-taper afterbodies reduce the normal force only slightly relative to the untapered one. On the other hand, afterbodies that also have taper of planform cause appreciable reduction in normal force. It is noticeable that the nonlinearity of the normal-force coefficient curves at large angles of attack increases by tapering the afterbody. This finding will be discussed in more detail in the following chapter.

Pitching-moment coefficient vs normal-force coefficient curves are presented in Figs. 4a and 4b. The slopes of the curves for configurations with tapered afterbodies are larger than that of the one with the cylindrical afterbody. This indicates a more forward center-of-pressure location at a fixed normal-force coefficient. As the angle of attack increases, the slopes of the curves decrease, indicating a backward shift in the center-of-pressure location.

Analysis and Discussion

Linear Aerodynamic Characteristics

The normal-force curve slope and the center-of-pressure location were obtained by fitting straight lines to the C_N vs α and C_m vs C_N curves, respectively, at small angles of attack. These stability derivatives are presented in Figs. 5a and 6a. The test results are compared with analytical predictions from an arbitrary slender-body code developed by Lapidot and Sigal.[3] The code uses the Schwartz-Christoffel transformation to transfer a polygonal approximation of the cross-sections of the body into circles. The Sacks[4] formulation of slender-body theory is used to evaluate the stability derivatives. The experimentally obtained normal-force curve slope is larger and the center of pressure more aft than those predicted. A similar

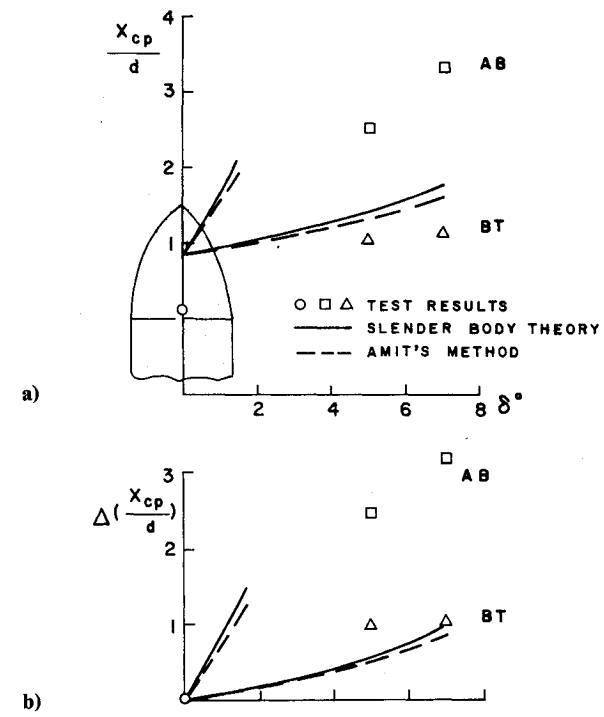

Fig. 6 Center-of-pressure location: a) the complete configurations; b) contribution of the afterbody.

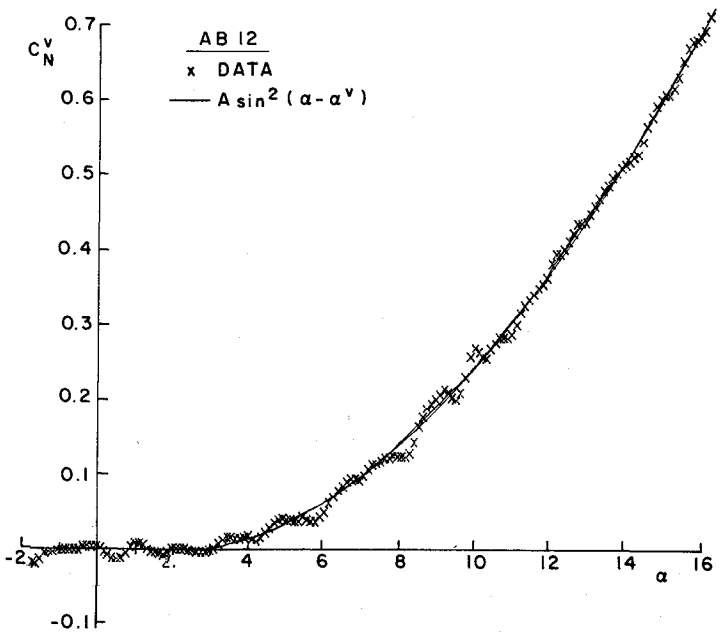

Fig. 7 Vortex-induced normal-force coefficient.

comparison for a matching circular body[2] having the same cross-sectional distribution as the present untapered model is summarized in Table 3. The two configurations show about the same disagreement between test results and analysis. It is concluded that the difference is not attributed to the shape of the cross-section but to the inability of slender-body theory to predict lift carryover on the cylindrical part of the body.

The contribution of the afterbodies to the normal-force curve slope was estimated by

$$\Delta C_{N_\alpha} = C_{N_\alpha} - C_{N_{\alpha_{AB10}}}$$

Experimentally obtained values for this contribution and predictions based on slender-body theory are shown in Fig. 5b. For the single-taper afterbodies, this contribution is small. The measured values for the double-taper afterbodies are about 22% smaller in absolute value than those predicted. Amit's method,[5] conceived for circular boattails, was also applied. The method suggests the use of equivalent taper, smaller than actual, to account for the thickening of the boundary layer on the afterbody. The use of this method reduces the gap between test results and analysis to about 12%.

Vortex-Induced Aerodynamic Characteristics

Examination of the test results at small angles of attack showed that nonlinearities in normal-force curves start beyond a typical threshold angle of attack. Therefore, a mathematical model containing such a threshold was selected to fit the test data. The model is similar to that of the DATCOM's[6] second method, which is a modified Polhamus[7] prediction for the vortex normal-force coefficient based on the leading-edge suction analogy

$$C_n^{\mathrm{v}} = A \sin^2(\alpha - \alpha^v) \quad , \quad \alpha > \alpha^v$$

The experimental vortex-induced normal-force coefficient is obtained by

$$C_{\mathrm{n}}^{\mathrm{v}} = C_N - \tfrac{1}{2} C_{N_\alpha} \sin 2\alpha$$

Figure 7 shows this data for the configuration having afterbody AB12. At small angles of attack, the data are scattered around the zero level, indicating that the vortex-induced contribution starts past a threshold.

The two parameters A and α^v were identified by curve fitting the model to the test data, and the results are presented in Fig. 8. The data for the parameter A show scatter but no discernible dependence on the geometry. On the other hand, the threshold angle of attack α^v decreases with increase of afterbody taper angle. The decrease in α^v means an earlier appearance of vortex normal force or a larger contribution at a fixed angle of attack.

Crossflow drag analogy such as that of Jorgensen[8] was used to estimate the coefficient A by

$$A = \eta C_{D_C} \frac{S_P}{S_R}$$

As no values for η for noncircular bodies were found, Jorgensen's correlation for circular bodies was used. Crossflow drag coefficient for a very similar geometry at subcritical Reynolds number was taken from Polhamus.[9] The estimated value of A is 11.0, being in good agreement with the average value of the test results.

The vortex-induced pitching-moment coefficient was obtained from the data in a similar way to that of the normal force:

$$C_{\mathrm{m}}^{\mathrm{v}} = C_m - \tfrac{1}{2} C_{m_\alpha} \sin 2\alpha$$

The center of pressure of the vortex-induced contribution is

$$X_{\mathrm{cp}}^{\mathrm{v}} = \frac{C_{\mathrm{m}}^{\mathrm{v}}}{C_{\mathrm{N}}^{\mathrm{v}}}$$

The results, presented in Fig. 9, show that at small angles of attack, $X_{\mathrm{c}}^{\mathrm{v}}\mathrm{p}$ is located at the aft end of the body. As the angle of attack increases, it moves forward, asymptotically approaching a fixed value that depends on afterbody geometry.

According to the crossflow analogy, the expected location of the vortex-induced center of pressure is

$$X_{cp}^{v} = \frac{-\ell_1 \int^{\ell n} C_{D_c} b x dx}{-\ell_1 \int^{\ell n} C_{D_c} b dx}$$

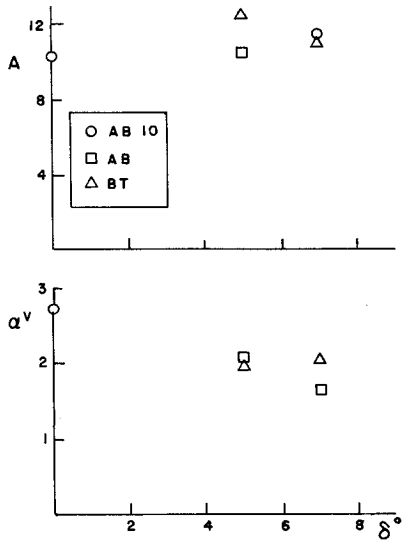

Fig. 8 Parameters of the model for vortex-induced normal-force coefficient.

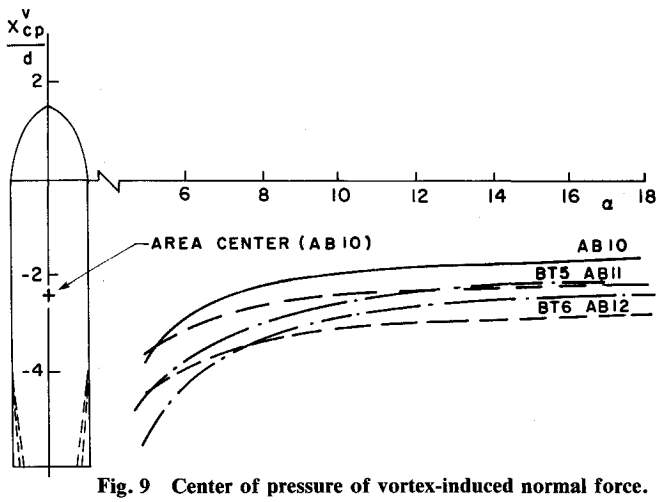

Fig. 9 Center of pressure of vortex-induced normal force.

For the case of constant C_{D_c}, this expression reduces to the center of projection area. In the present models, the corners of the nose are sharp, whereas those of the centerbody and the afterbodies are rounded. The data of Ref. 9 were used in the evaluation of $X^v_c p$, and the results are shown in Fig. 9. For the configuration with $AB10$, the experimentally obtained $X^v_c p$ at angles of attack larger than 15 deg is about 0.6 reference lengths ahead of the predicted location. Adding taper to the afterbody shifts the asymptotic value of $X^v_c p$ backward. For the configuration with afterbody $AB12$, the experimentally obtained location at angles of attack larger than 15 deg is about 0.5 reference lengths more aft than predicted.

Conclusions

A model of a rectangular cross-sectional body with rounded corners and five interchangeable afterbodies was tested at a Mach number of 0.85 and angles of attack up to 18 deg. The normal-force curve slope of the configuration with an untapered afterbody is larger and the center of pressure location is more aft than predicted by slender-body theory. The differences between the experimental linear characteristics and the predicted ones are very close to those found for matching circular bodies.

Afterbody taper in thickness and width causes a reduction in the normal-force curve slope and a forward shift in the center-of-pressure location. The amount of reduction in the normal-force curve slope is about 22% lower than that predicted by slender-body theory and about 12% lower than that predicted by Amit's equivalent taper method.

Afterbody taper increases the vortex-induced normal force by reducing the threshold angle-ofattack for its initiation. The center of pressure of this contribution is located at the aft end of the body at small angles of attack, and it asymptotically moves forward, approaching a fixed location as the angle of attack increases. Afterbody taper shifts the location of the center of pressure of the vortex-induced contribution backward, in spite of the forward shift in the center of projection area.

Acknowledgments

Initial support for this work was provided by the Aerodynamic Laboratory headed by Profs. D. Weihs and A. Seginer. Additional funding was provided by RAFAEL under Contract 46/0420/6. The contract monitor was Mr. Z. Shpond. The test engineers were Dr. M. Victor and Mr. E. Shaskin. Data reduction was done by Mr. M. Neiger and Mr. N. Sigal, using a code written by Mr. S. Menashe.

References

[1]Jackson, C. M., Jr. and Sawyer, W. C., "Bodies with Noncircular Cross-Sections and Bank-to-Turn Missiles," *Tactical Missile Aerodynamics*, edited by M. J. Hemsch, and J. N. Nielsen, *Progress in Astronautics and Aeronautics*, Vol. 104, AIAA, New York, 1986.

[2]Sigal, A., "An Experimental Investigation of the Aerodynamic Characteristics of Bodies Having Square Cross-Section at Transonic Speeds," AIAA Paper 84-2091, Aug. 1984.

[3]Lapidot, E. and Sigal, A., "An Interactive Software for Preliminary Aerodynamic Design of Slender Bodies Having Arbitrary Cross-Sections," *Proceedings of the 29th Israel Conference on Aviation*, Haifa, Israel, Feb. 1987.

[4]Sacks, A. H., "Aerodynamics Forces, Moments and Stability Derivatives for Slender Bodies of General Cross-Section," NACA TN-3283, Nov. 1954.

[5]Amit, N., "An Experimental Investigation of the Lift and Pitching-Moment of Configurations Having Boattails With and Without Fins," M.Sc. Thesis, Technion, March 1973.

[6]*DATCOM—Stability and Control Handbook*, 2nd ed., USAF, Flight Dynamics Lab., Wright-Patterson AF Base, Ohio, 1975.

[7]Polhamus, E. C., "A Concept of the Vortex Lift of Sharp Edge Delta Wings Based on Leading-Edge-Suction Analogy," NASA TN-D-3767, July 1966.

[8]Jorgensen, L. H., "Prediction of Static Aerodynamic Characteristics for Slender Bodies Alone and With Lifting Surfaces to Very High Angles of Attack," NASA TR-R-474, Sep. 1977.

[9]Polhamus, E. C., "A Review of Some Reynolds Number Effects Related to Bodies at High Angles of Attack," NASA CR-3809, Aug. 1984.